

# Multiferroic Properties of Pure and Transition Metal Doped LaFeO<sub>3</sub> Nanoparticles

Iliana Naumova Apostolova, Angel Todorov Apostolov, Steffen Trimper,\*  
and Julia M. Wesselinowa

The size, doping concentration, and magnetic field dependences of the magnetization  $M$  and the real part of the dielectric function  $\epsilon'$  in doped LaFe<sub>1-x</sub>M<sub>x</sub>O<sub>3</sub> nanoparticles (NPs) are studied using a microscopic model. Although  $M$  increases,  $\epsilon'$  decreases with decreasing NPs size in pure LaFeO<sub>3</sub>. Doping with different ions causes different strain which modifies the exchange interaction. As a consequence,  $M$  and  $\epsilon'$  grow with increasing Mn or Zn ion doping, whereas both quantities decrease by doping with Ti or Al ions. The magneto-dielectric coefficient increases with an applied external magnetic field and Mn doping concentration in pure and Mn-doped LaFeO<sub>3</sub> indicating that pure and doped LaFeO<sub>3</sub> NPs exhibit a multiferroic behavior. A microscopic model is proposed to study multiferroic Bi<sub>2</sub>NiMnO<sub>6</sub> thin films.

Neel temperature as first reported by Acharya et al.<sup>[2]</sup> Such a multiferroic behavior was confirmed also by Bhargava et al.<sup>[3]</sup> The temperature dependence of  $\epsilon$  of pure LFO exhibits maxima similar to the ones observed in ferroelectric ceramics with non-centrosymmetric point group.<sup>[3]</sup> Moreover, orthorhombically distorted LFO shows G-type weak antiferromagnetic ordering below  $T_N = 740$  K and a transition to ferroelectric ordering at  $T_C = 475$  K.<sup>[4]</sup> The magnetoelectric properties can be intensified by doping with transition metal ions; see refs. [5–9] Ion doping of LFO nanoparticles (NP) induces a transition from an antiferromagnetic to a weak ferromagnetic behavior.

Size effects in LFO-NP are studied experimentally by Qiu et al. and Thirumalairajan et al.<sup>[10,11]</sup> The weak ferromagnetic behavior in LFO-NP is attributed to uncompensated spins at the surface as reported by Phokha et al.<sup>[12]</sup> Bulk LFO is an antiferromagnet contrary to the weak ferromagnetism in NP form.

The motivation of our article consists of the observation that such perovskite-type oxides of ABO<sub>3</sub> type have aroused several applications in many areas such as advanced materials, magnetic storage media, sensors, catalysis, and solid-state chemistry due to their variable structural, chemical composition, and magneto-electric coupling effect. Because the applicability of LFO compounds depends strongly on their electric, magnetic and optical properties, it seems to be decisive to study the influence of the material characteristics. One of the possibilities to enhance the properties of LFO is ion doping or partial substitution to cause valence alternation or oxygen vacancies. Moreover, doped LFO shows oxygen ion conductivity and has been studied for its applications in oxygen-permeable membrane catalytic activity, as well as being used as sensors, utilized in microwave dielectrics and as solid electrolytes. As demonstrated recently,<sup>[13]</sup> ion doping affects the optical properties by decreasing the bandgap with increasing Co doping. In addition, NPs may show unusual magnetic properties due to the finite-size effects, surface anisotropy effects, interface effects, or shape anisotropy effect. As already mentioned, bulk LFO exhibits antiferromagnetic behavior, whereas the NPs show ferromagnetic behavior with pronounced hysteresis loops.

Until now, the investigation of ion doping and size effects in LFO is still missing, in particular, within a microscopic model. Using first-principle calculation, Weingart et al.<sup>[14]</sup> have investigated the mechanisms leading to weak ferromagnetism in LFO.

## 1. Introduction


Multiferroic behavior in the same phase is widely discussed.<sup>[1]</sup> Rare earth orthoferrite such as LaFeO<sub>3</sub> (LFO) with an ABO<sub>3</sub> structure is technically important due to its structural, optical, electrical, and magnetic properties. Measuring the dielectric constant  $\epsilon$  in the presence and absence of magnetic fields, the orthorhombically distorted perovskite LFO is a multiferroic material with a high

Dr. I. N. Apostolova  
University of Forestry  
1756 Sofia, Bulgaria

Dr. A. T. Apostolov  
Department of Physics  
University of Architecture, Civil Engineering and Geodesy  
1046 Sofia, Bulgaria

Prof. S. Trimper  
Institute of Physics  
Martin-Luther-University  
Von-Seckendorff-Platz 1, 06120 Halle, Germany  
E-mail: steffen.trimper@physik.uni-halle.de

Prof. J. M. Wesselinowa  
Department of Physics  
University of Sofia  
Blvd. J. Bouchier 5, 1164 Sofia, Bulgaria

 The ORCID identification number(s) for the author(s) of this article can be found under <https://doi.org/10.1002/pssb.202000482>.

© 2020 The Authors. Published by Wiley-VCH GmbH. This is an open access article under the terms of the Creative Commons Attribution License, which permits use, distribution and reproduction in any medium, provided the original work is properly cited.

DOI: 10.1002/pssb.202000482

Mao et al.<sup>[15]</sup> have studied the structural phase transition and the spin reorientation of LFO, whereas Pushpa et al.<sup>[16]</sup> had been interested in the electronic properties of Ca-doped LFO. The magnetic properties of bulk LFO are studied<sup>[17–20]</sup> by applying the Heisenberg model.

Based on our previous articles concerning the multiferroic properties of BiFeO<sub>3</sub> (BFO),<sup>[21,22]</sup> the aim of the present one is the consideration of the multiferroic properties of pure and transition-metal-doped LFO-NP within a microscopic model. The difference in both materials is that bulk BFO offers a multiferroic behavior contrary to the para-electric antiferromagnet LFO. It offers a canted G-type antiferromagnetic structure with a high Neel temperature of  $T_N = 740$  K. The Fe<sup>3+</sup> spins are coupled antiferromagnetically with opposite spin direction between two sub-lattices.

## 2. The Model

As already discussed by Apostolov et al.,<sup>[22]</sup> the Hamiltonian describing the magnetic properties of transition-metal  $M$ -doped LFO, LaFe<sub>1-x</sub>M<sub>x</sub>O<sub>3</sub> reads

$$\begin{aligned}
 H_m = & -\frac{1}{2} \sum_{\langle ij \rangle} (1-x) J_{1ij}^{\text{Fe-Fe}} S_i^{\text{Fe}} \cdot S_j^{\text{Fe}} \\
 & -\frac{1}{2} \sum_{[ij]} J_{2ij}^{\text{Fe-Fe}} S_i^{\text{Fe}} \cdot S_j^{\text{Fe}} - K \sum_i (S_i^{\text{zFe}})^2 \\
 & - \sum_{ij} D_{ij}^{\text{Fe-Fe}} \cdot (S_i^{\text{Fe}} \times S_j^{\text{Fe}}) - g\mu_B h \cdot \sum_i S_i^{\text{Fe}} \\
 & -\frac{1}{2} \sum_{\langle ij \rangle} x J_{ij}^{\text{Fe-M}} S_i^{\text{Fe}} \cdot S_j^{\text{M}}
 \end{aligned} \quad (1)$$

where  $S_i$  is the spin operator at site  $i$ . The exchange integral  $J_1 = J_{ab} = J_c < 0$  represents the coupling between the nearest neighbor Fe spins along the ab-plane and the c-axis, which are assumed to be equal.<sup>[17,18]</sup> The next-nearest neighbor coupling is assumed  $J_2 < 0$ . The underlying R3c symmetry permits a canting of the antiferromagnetic sub-lattices. Such a canting of the Fe<sup>3+</sup> spins is directly related to the antisymmetric Dzyaloshinskii–Moriya (DM) exchange interaction  $D_{ij}^{\text{Fe-Fe}}$ <sup>[14,17,22]</sup>. The single-ion anisotropy of the Fe ion along the z-axis is  $K^{\text{Fe}} > 0$  and  $h$  is the external magnetic field. The last term in Equation (1) includes the interaction between the Fe and the transition-metal-doped ions. As La<sup>3+</sup> is nonmagnetic, one gets  $J^{\text{La-Fe}} = 0$ .

The two aspects of the system, namely the magnetic as well as the dielectric properties are analyzed using Green's function techniques. The magnetic behavior is deduced from the spin Green's function  $g_{ij} = \langle \langle S_i^+; S_j^- \rangle \rangle$  and leads to the magnetization  $M$  for arbitrary spin  $S$

$$M = \frac{1}{N} \sum_i [(S + 0.5) \coth[(S + 0.5)\beta E_{mi}] - 0.5 \coth(0.5\beta E_{mi})] \quad (2)$$

Here,  $E_{mi}$  is the magnetic spin wave energy at site  $i$ .

Concerning the ferroelectricity, let us emphasize that the appearance of a room temperature polarization hysteresis in

LFO is triggered by the canted spin of the Fe ions, in contrary to BFO, where the polarization is due to the shift of Bi ions with respect to the FeO<sub>6</sub> octahedrons.<sup>[22]</sup>

Following<sup>[23]</sup> the energy-dependent dielectric function  $\epsilon(E)$  obeys

$$\left[ \left( \frac{\Lambda}{\epsilon(E) - 1} \right)_{\alpha\gamma} + \Lambda \frac{k_\alpha k_\gamma}{k^2} \right] G^{\gamma\beta}(k, E) = \delta_{\alpha\beta} \quad (3)$$

with  $\Lambda = 4\pi Z^2/\nu$  and  $Z$  is the electron charge,  $\nu$  is the volume, and the indices  $\alpha, \beta, \gamma$  are the components of the related spins. In the present situation, one needs the longitudinal anticommutator Green's function with for instance  $\alpha = z$   $G^{zz}(E) = \langle \langle B_i^z; B_j^z \rangle \rangle$  for appropriate pseudospin-operators  $B_i$  within the transverse Ising model.<sup>[22]</sup> The method introduced in ref. [24] gives

$$G_{ij}^{zz}(E) = \frac{2\langle B_i^z B_j^z \rangle (E^2 - (E_{fi})^2 + 2iE\gamma^{11})}{(E + i\gamma^{33})(E^2 - (E_{fi})^2 + 2iE\gamma^{11}) - E(\epsilon^{13})^2} \quad (4)$$

Notice that the elementary excitation and their damping determine the dielectric properties of the system. Here  $E_{fi}$  and  $\gamma^{11}$  are the related transverse pseudo-spin-wave energy at lattice site  $i$  and its damping, whereas  $\gamma^{33}$  is the damping of the longitudinal mode and  $\epsilon^{13}$  characterizes the coupling between the longitudinal and transverse modes. The damping coefficients contribute to the imaginary part of the dielectric function which is not considered in the present article.

## 3. Numerical Results and Discussion

For the numerical evaluation of our analytical finding of ion-doped LFO, LaFe<sub>1-x</sub>M<sub>x</sub>O<sub>3</sub>, we use the following model parameters:  $J_1^{\text{Fe-Fe}} = -5.47$  meV,  $J_2^{\text{Fe-Fe}} = -0.24$  meV,  $J = -0.24$  meV,  $K^{\text{Fe}} = 0.0037$  meV,  $D^{\text{Fe-Fe}} = 0.0124$  meV,<sup>[17]</sup>  $J_d^{\text{Fe-Mn}} = 7.5$  meV,<sup>[25]</sup>  $J_d^{\text{Fe-Ti}} = 3.45$  meV<sup>[26]</sup>  $S = 2.5$ . The LFO-NP offer a shell structure numbered by  $n = 1, \dots, N$ , where  $n = 1$  is the central spin and  $n = N$  corresponds to the surface shell.

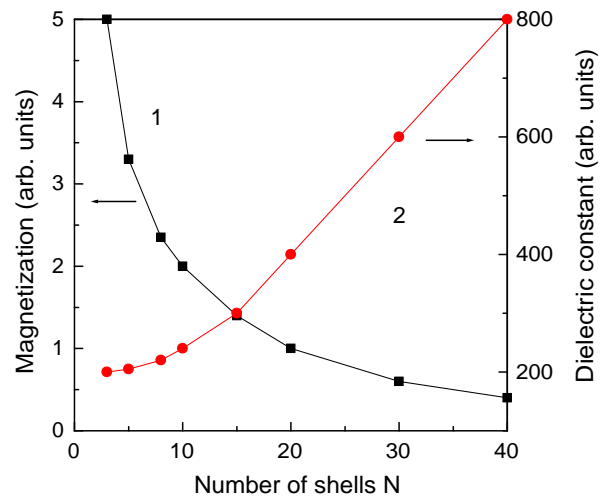


**Figure 1.** Size dependence of the magnetization  $M$  (1) and the dielectric constant (2) of a pure LFO-NP at room temperature.

The size dependence of the magnetization and dielectric constant of pure LFO-NP at room temperature is shown in **Figure 1**, curve 1. As emphasized before, the NP exhibit a weak ferromagnetism due to spin-canted iron moments generated from disordered surface spins. The magnetization grows up with decreasing NP size which is observed by Qiu et al.<sup>[10]</sup> The increase in the real part of the dielectric constant  $\epsilon'$  with increasing NP size, see curve 2 in **Figure 1**, is also in accordance with experimental observation in ref. [10]

In **Figure 2**, we present the influence of transition metal ion doping, for example, Mn-doped LFO-NP  $\text{LaFe}_{1-x}\text{Mn}_x\text{O}_3$  with  $x = 0 - 0.5$ . Doping of ions with different radius compared with the Fe ion leads to different strains. As a consequence of defects, denoted by the index  $d$ , the model parameters are changed because the interaction constants depend on the distance between the ions. So  $J$  is proportional to the inverse of the distance between two nearest spins. The radius of the Mn ion is smaller compared with that of the Fe ion, i.e., there appears a compressive strain and the lattice parameters decrease.<sup>[5,8]</sup> From here, we conclude  $J_d > J_b$ . The magnetization  $M$  for a Mn-doped LFO-NP is shown as curve 1 in **Figure 2**. One observes an increase in  $M$  due to an enhanced Mn doping concentration  $x$ . The result is in agreement with experimental data.<sup>[5,8]</sup> The ferromagnetism is due to defective states at the surface and due to the strong  $\text{Mn}^{3+}/\text{Fe}^{3+}$  exchange interactions. In addition, the Mn ion doping has an influence on the real part of the dielectric constant  $\epsilon'$  which is shown in **Figure 3**, curve 1. Here  $\epsilon'$  in doped LFO-NP increases with increasing Mn doping concentration  $x$ . The result is again in good qualitative agreement with the experimental data offered in ref. [5] and in ref. [8].

In case of multiferroic materials, the dielectric constant  $\epsilon'$  is affected by the magnetic ordering generated by an applied magnetic field  $h$ . To demonstrate this effect, we have calculated  $\epsilon'$  of Mn-doped LFO-NP in the presence of external magnetic fields in the range  $h = 0 - 10$  kOe. In particular, we are interested in the magneto-dielectric coefficient (MD), defined by

$$\text{MD} (\%) = (\epsilon'(h) - \epsilon'(h = 0)) / \epsilon'(h = 0) \quad (5)$$

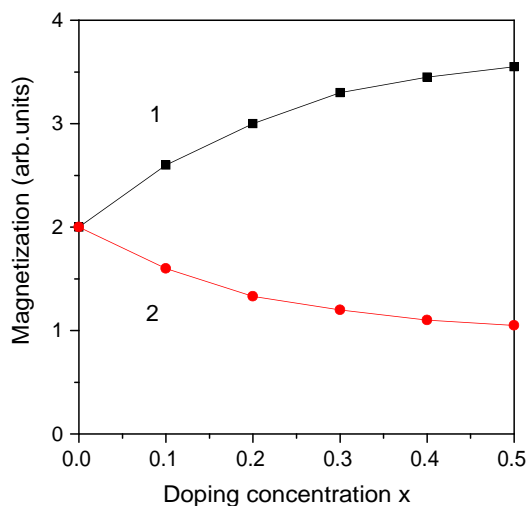


**Figure 2.** Magnetization  $M$  of LFO-NP under doping: Mn (1); Ti (2);  $T = 300$  K,  $N = 10$  shells.

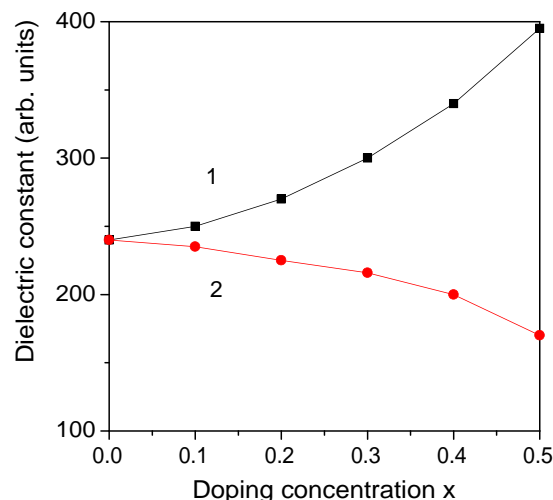


**Figure 3.** Dielectric constant  $\epsilon'$  under doping by Mn (1) and Ti (2);  $T = 300$  K,  $N = 10$  shells.

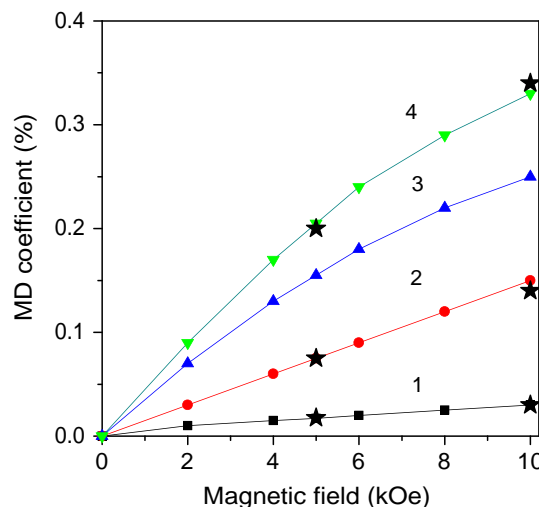


**Figure 4.** MD defined in Equation (5), of doped LFO-NP for different Mn concentration:  $x = 0$  (1); 0.1 (2); 0.3 (3); 0.5 (4). The black stars are experimental data from ref. [5];  $N = 15$  shells,  $T = 300$  K.

The MD, shown in **Figure 4**, increases with increasing magnetic field  $h$ . Clearly, there exists a strong magneto-dielectric coupling, indicating that pure and Mn ion doped LFO-NP are multiferroics.<sup>[2,3,5]</sup>

The increase in the MD could be originated by an enhanced lattice strain, caused by surface and size effects or by ion doping, as well as due to a magnetostriction effect. The MD for different doping concentrations,  $x = 0 - 0.5$  is shown in **Figure 4**. One realizes an increase with increasing concentration  $x$ . The experimental data for 5 and 10 kOe are taken from ref. [5] The surprising good agreement between our results and the experimental data seems to be a confirmation for choosing the model in Equation (1).

A similar behavior, namely an enhancement of  $\epsilon'(x)$  is observed by Zn doping concentration  $x$  in a Zn-doped LFO-NP.

The ionic radius of the  $\text{Zn}^{2+}$  ions is smaller compared with the  $\text{Fe}^{3+}$  ions and consequently the induced compressive strain leads again to an increase in the exchange interaction  $J_d$  in analogy to Mn-doped LFO-NP. The raise of  $\epsilon'$  with increasing Zn doping ions is discovered experimentally, see ref. [6].

As a last point, we demonstrate that doping with Ti ions leads to a decrease in  $\epsilon'$ . As the  $\text{Ti}^{4+}$  ionic radius of 0.61 Å is greater than that of  $\text{Fe}^{4+}$  (0.58 Å), there appears a tensile strain which is related to an increase in the lattice parameters. Accordingly, this leads to  $J_d < J_b$ . Moreover, the substitution of magnetic  $\text{Fe}^{3+}$  ions by nonmagnetic  $\text{Ti}^{4+}$  ions can reduce the exchange interaction between neighbor spins. The calculations lead to a decrease in the magnetization with increasing Ti ion concentration  $x$ . The results for  $x > 0.2$  are presented in Figure 2, curve 2. Using our Green's function approach, we find also the dielectric constant depending on the Ti concentration. Curve 2 in Figure 3 shows that  $\epsilon'$  decreases with increasing  $x$ . Such a result is likewise in agreement with experimental data offered in ref. [7]. A similar behavior is also obtained for Al-doped LFO-NP where a tensile strain is occurred as reported in refs. [27,28]. We have calculated the MD also for Ti-doped LFO and observe an increase with increasing magnetic field  $h$ , although it decreases with increasing Ti doping concentration  $x$  (Figure 3). A similar behavior is observed in LFO doped with Zn at the La site in ref. [29], where the MD decreases with increasing Zn doping, but increases with increasing  $h$ . Another result is due to ref. [30] where it had been reported that MD in Ti and Al co-doped LFO is also positive, and as well increases with growing magnetic field  $h$ . Notice that the MD increases with  $h$  in pure LFO,<sup>[2,3]</sup> too. This indicates the existence of positive coupling between magnetic and electric order parameter in the samples at room temperature.

Summarizing our calculations, we have demonstrated that the modified Heisenberg model defined in Equation (1) enables us the description of the size, doping concentration, and magnetic field dependence of the magnetization  $M$  as well the real part of the dielectric constant  $\epsilon'$  in transition-metal-doped LFO,  $\text{LaFe}_{1-x}\text{M}_x\text{O}_3$  NP. In particular, let us highlight the good quantitative agreement of the MD defined in Equation (5) with the experimental data in ref. [5].

## Acknowledgements

Open access funding enabled and organized by Projekt DEAL.

## Conflict of Interest

The authors declare no conflict of interest.

## Keywords

dielectric function,  $\text{LaFeO}_3$  nanoparticles, magnetization, microscopic models, transition-metal doping

Received: September 3, 2020  
Revised: September 22, 2020  
Published online: October 19, 2020

- [1] M. Fiebig, *J. Phys. D: Appl. Phys.* **2005**, *38*, R123.
- [2] S. Acharya, J. Mondal, S. Ghosh, S. K. Roy, P. K. Chakrabarti, *Mater. Lett.* **2010**, *64*, 415.
- [3] K. K. Bhargava, S. Ram, S. B. Majumdera, *J. Appl. Phys.* **2014**, *115*, 204109.
- [4] M. Idrees, M. Nadeem, M. Atifc, M. Siddique, M. Mehmood, M. M. Hassan, *Acta Mater.* **2011**, *59*, 1338.
- [5] S. K. Kundu, D. K. Rana, L. Karmakar, D. Das, S. Basu, *J. Mater. Sci.: Mater. Electron.* **2019**, *30*, 10694.
- [6] S. Manzoor, S. Husain, A. Somvanshi, M. Fatema, N. Zarrin, *J. Mater. Sci.: Mater. Electron.* **2019**, *30*, 19227.
- [7] C. Sasikala, N. Durairaj, I. Baskaran, B. Sathyaseelan, M. Henini, E. Manikan, *J. Alloys Compd.* **2017**, *712*, 870.
- [8] G. Anjum, R. Kumar, S. Mollah, D. K. Shukla, S. Kumar, C. G. Lee, *J. Appl. Phys.* **2010**, *107*, 103916.
- [9] P. Shikha, T. S. Kang, B. S. Randhawa, *RSC Adv.* **2015**, *5*, 96799.
- [10] Y. Qiu, Y. S. Luo, Z. J. Zou, Z. M. Tian, S. L. Yuan, Y. Xi, L. Z. Huang, *J. Mater. Sci.: Mater. Electron.* **2014**, *25*, 760.
- [11] S. Thirumalairajan, K. Girija, V. R. Mastelaro, N. Ponpandian, *J. Mater. Sci.: Mater. Electron.* **2015**, *26*, 8652.
- [12] S. Phokha, S. Pinitsoontorn, S. Maensiri, S. Rujirawat, *J. Sol-Gel Sci. Technol.* **2014**, *71*, 333.
- [13] S. Subudhi, A. Mahapatra, M. Mandal, S. Das, K. Sa, I. Alam, B. V. R. S. Subramanyam, J. Raiguru, P. Mahanandia, *Integr. Ferroelectr.* **2020**, *205*, 61.
- [14] C. Weingart, N. Spaldin, E. Bousquet, *Phys. Rev. B* **2012**, *86*, 094413.
- [15] A. J. Mao, H. Tian, X. Y. Kuang, J. W. Jia, J. S. Chai, *RSC Adv.* **2016**, *6*, 100526.
- [16] R. Pushpa, D. Daniel, D. Butt, *Solid State Ionics* **2013**, *249*, 184.
- [17] K. Park, H. Sim, J. C. Leiner, Y. Yoshida, J. Jeong, S. Yano, J. Gardner, P. Bourges, M. Klicpera, V. Sechovsky, M. Boehm, J. Park, *J. Phys.: Condens. Matter* **2018**, *30*, 235802.
- [18] R. J. McQueeney, J. Q. Yan, S. Chang, J. Ma, *Phys. Rev. B* **2008**, *78*, 184417.
- [19] B. H. Kim, B. I. Min, *New J. Phys.* **2011**, *13*, 073034.
- [20] Y. M. Abbas, A. B. Mansour, S. E. Ali, A. H. Ibrahim, *J. Adv. Phys.* **2018**, *14*, 5664.
- [21] J. M. Wesselinowa, I. Apostolova, *J. Appl. Phys.* **2008**, *104*, 084108.
- [22] A. T. Apostolov, I. N. Apostolova, S. Trimper, J. M. Wesselinowa, *Solid State Commun.* **2019**, *300*, 113692.
- [23] V. G. Vaks, *Introduction to the Microscopic Theory of Ferroelectrics*, Nauka, Moscow **1973**, p. 158.
- [24] Yu. A. Tserkovnikov, *Teor. Mat. Fiz.* **1971**, *7*, 250.
- [25] M. A. Zagrebina, V. V. Sokolovskiy, V. D. Buchelnikov, M. A. Klyuchnikova, *Phys. Proc.* **2015**, *75*, 1427.
- [26] K. A. Misbach-ul-Islam, K. H. Hashmi, M. U. Rana, T. Abbas, *Solid State Commun.* **2002**, *121*, 51.
- [27] J. M. Wesselinowa, *J. Magn. Magn. Mater.* **2010**, *322*, 234.
- [28] W. Ni, J. Ye, Y. Guo, C. Cheng, Z. Lin, Y. Li, H. Wang, Y. Yu, Q. Li, S. Huang, Z. Shao, C. Wang, *J. Am. Ceram. Soc.* **2017**, *100*, 3042.
- [29] K. Mukhopadhyay, A. S. Mahapatra, P. K. Chakrabarti, *J. Magn. Magn. Mater.* **2013**, *329*, 133.
- [30] A. Mitra, A. Shaw, P. K. Chakrabarti, *Adv. Powder Technol.* **2020**, *31*, 2469.